International Journal of Mechatronics and Applied Mechanics
2025, Issue 20, Vol. 1

RESEARCH ON THE INFLUENCE OF DRIVING MODE ON DYNAMIC CHARACTERISTICS OF ON-BOARD SHORT-DISTANCE SCRAPER CONVEYOR

Gao Ranhang [1], Zhang Hong[1], Yang Lu[1], Feng Qian[1], and Yuan Wenyu[1]*
[1]School of Mechanical Engineering, Taiyuan University of Science and Technology, Taiyuan 030024, P.R.China

Abstract - The driving modes of on-board short-distance scraper conveyors in roadway tunneling equipment exhibit significant diversity, with different configurations inducing distinct variations in operational resistance and acceleration impacts, ultimately influencing the transport efficiency and service life of the conveying system. To address this issue, this study focuses on the on-board short-distance scraper conveyor integrated with a roadheader-bolter. Kinematic and dynamic models of the scraper chain transmission system are derived, and a multi-body contact dynamics model is established by defining the topological relationships among components under realistic operating conditions. The dynamic characteristics of the conveyor are systematically investigated under two driving modes—head-end drive and tail-end drive—with emphasis on the effects of conveyor inclination angle and chain speed. The results demonstrate that: The acceleration impact at the chain-sprocket meshing zone exhibits a positive correlation with both the inclination angle and chain speed, while the dynamic variation of the driving torque follows a distinctive "pentagram-shaped" distribution pattern; Under tail-end drive mode, the acceleration impact at the meshing zone is slightly higher compared to head-end drive, whereas head-end drive shows particularly pronounced sensitivity of driving torque to fluctuations in chain speed; Tail-end drive effectively suppresses shock induced by abrupt torque variations, thereby enhancing operational stability. These findings provide critical insights for optimizing drive configurations and operational parameters in practical engineering applications.

Keywords: Roadway excavation equipment, On-board short-distance scraper conveyor, Running resistance, Driving modes, Acceleration impact.

1. Introduction

In coal mine roadway excavation, widely used tunneling equipment includes roadheaders, boom-type shearers, and continuous miners[14]. Such equipment employs short-distance scraper conveyor technology in their haulage units responsible for transporting coal materials. The function of these conveyors is to transfer the coal particles collected by the gathering arms to the secondary transfer equipment behind the conveyor.The driving modes of haulage units vary across different equipment. For instance, the EML340 continuous miner typically adopts a head-end driving configuration, with the power required by the loading unit integrated and driven by the same motor. In contrast, the EJM340 roadheader-integrated bolter employs an independent tail-end motor drive. Currently, there is no standardized specification for the driving modes of haulage units. Under different chain speeds and conveying angles, the driving mode affects the operational resistance, and acceleration impacts on the haulage unit, thereby influencing the service life and transportation efficiency of the tunneling equipment.

In the study of dynamic characteristics and trough wear of scraper conveyors in fully mechanized mining faces, Wang et al.[11] established a rigid-flexible coupled nonlinear dynamic model of the scraper chain and sprocket to analyse the influence of sprocket tooth count and load on the chain drive system, while Wang et al.[12] designed an impact load testing scheme for the middle plate of conveyor trough to investigate wear effects of scrapers and chains on different plate regions. Ma et al. [5] further analysed scraper dynamics and trough wear characteristics based on a

https://doi.org/10.17683/ijomam/issue20.22

coupled conveyor model. Regarding chain drive mechanisms, Wang et al. [9] developed a rigid-flexible coupled contact dynamics model for tail-end chain drives to examine load-start dynamics and contact stress responses of round-link chains and sprockets, whereas Wang et al. [10] established a roller chain dynamics model to explore high-speed impact behaviours. He [3] specifically investigated three-body wear characteristics of chain links under various abrasive conditions. For structural interactions, Song et al. [7] analysed displacement, angular and velocity variations between adjacent troughs in curved sections along with contact force characteristics at bell-shaped connections, and Zhao [15] employed discrete element modelling to study coal particle stratification and differential trough wear during transport. In shortwall mining applications, Yang et al. [13] modelled continuous miner scraper chains to develop cyclic dynamic load analysis methods, while Jiang [4] conducted component design and selection for on-board short-distance scraper conveyors. Complementing these studies, Gao [1] systematically examined meshing force and tension variations during chain-sprocket engagement processes. These collective investigations provide comprehensive insights into the dynamic behaviours, wear mechanisms and operational optimization of scraper conveyor systems under various mining conditions.

In summary, while research on various types of scraper conveyors in fully mechanized mining faces has reached a relatively mature stage, further investigation is still required regarding the operational performance of on-board short-distance scraper conveyors in roadway development faces. Currently, the selection criteria for drive configurations of such equipment remain ambiguous and lack standardized specifications.

To address this gap, this study derives kinematic and dynamic models of the scraper chain transmission system. A multi-body dynamic model of the on-board short-distance swing-type scraper conveyor system was established using SolidWorks and RecurDyn software. The research systematically examines and analyzes the influence of different drive modes on the periodic dynamic characteristics of the conveyor under various operational conditions, including different inclination angles and chain speeds. Through comparative analysis, the study quantifies the acceleration impacts at the chain-sprocket meshing interface during cyclic operation and characterizes the dynamic variation patterns of driving sprocket torque across different drive configurations. The findings of this research provide a theoretical foundation for the optimal selection of drive systems in short-distance scraper conveyors for roadway development equipment.

2. Kinematics of Scraper Chain Drive

2.1 Polygon Effect of Scraper Chain

The onboard short-distance scraper conveyor employs a sleeve roller chain formed by interconnecting chain links via pin shafts. During operation, the sprocket teeth engage with corresponding chain links to transmit power. Due to the finite number of sprocket teeth, the engaged chain segment forms a portion of a regular polygon, creating a polygonal effect in the transmission process. This phenomenon generates fluctuating velocities at the meshing points, consequently inducing vibrations in the conveyor system. As illustrated in Figure 1, the chain centerline alternates between tangent and secant positions relative to the sprocket's pitch circle (with radius r) during operation. When the drive sprocket rotates at constant angular velocity, the linear velocity of the scraper chain exhibits periodic variations and fluctuations relative to the sprocket's angular speed[13].

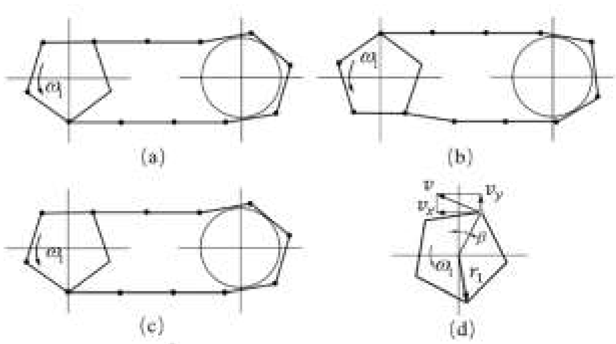

Figure 1: Schematic diagram of chain polygon effect

The average speed of the chain is:

$$v_m = \frac{z_1 \times p \times n_1}{60 \times 1000} \tag{1}$$

Where z_1 is the number of teeth of the sprocket; p is the pitch of the chain, mm; $n_1$is the speed of the sprocket, r/min.

When the driving sprocket rotates with a constant angular velocity ω_1, the kinematic analysis of the engaging chain link's hinge at positions a, b, and c in Figure 1 reveals the following velocity components:

$$v_x = r_1\omega_1 \cos\beta, \quad v_y = r_1\omega_1 \sin\beta \tag{2}$$

During operation, the chain exhibits vertical oscillations perpendicular to the centreline while simultaneously experiencing velocity fluctuations along the centreline direction. These kinematic variations lead to vibrational impacts and additional dynamic loads on the system. The acceleration along the chain's centreline direction is given by:

$$a = \frac{dv_x}{dt} = \frac{dr_1\omega_1 \cos\beta}{dt} = -r_1\omega_1^2 \sin\beta \tag{3}$$

The change of the chain speed can be expressed by the chain speed non-uniformity coefficient K_t:

$$K_t=\frac{v_{x\max}-v_{x\min}}{v_m}=\frac{r_1\omega_1\left(1-\cos\frac{180^\circ}{z_1}\right)}{r_1\omega_1\left(1+\cos\frac{180^\circ}{z_1}\right)\Big/2}=2tg^2\frac{90^\circ}{z_1} \quad (4)$$

Through in-depth analysis, it can be observed that the magnitude of the non-uniformity coefficient is closely related to the number of teeth on the drive sprocket. Specifically, when the sprocket has fewer teeth, the polygon effect becomes more pronounced, which directly leads to greater disturbances in the stability of the entire conveying system, thereby adversely affecting its smooth operation.

2.2 Impact Characteristics at the Engagement of Scraper Chain

The on-board short-distance scraper conveyor system is subject to polygon effect-induced impacts of varying magnitudes under different drive configurations. Taking the conveying system of a roadheader-bolter as an example, when the scraper chain operates at constant cyclic speed during its engagement with the five-tooth drive sprocket, the chain segment elevates from the lowest engagement point i to the highest point i_0 through rotation angle β . This movement causes expansion of the spacing between inner and outer knuckle joints, resulting in subsequent pitch elongation.

During this process, the actual engagement trajectory deviates inward from the theoretical path (as illustrated in Figure 2, transitioning from c_0-i-b_0-a_0 to c_0-j_0-i_0-b_0-a_0). The rapid convergence of pitch circle radius reduction Δr to 0 triggers chain engagement impact acceleration. Concurrently, the chain velocity undergoes significant abrupt changes and sustains repeated severe impact loads throughout the continuous rotation process.

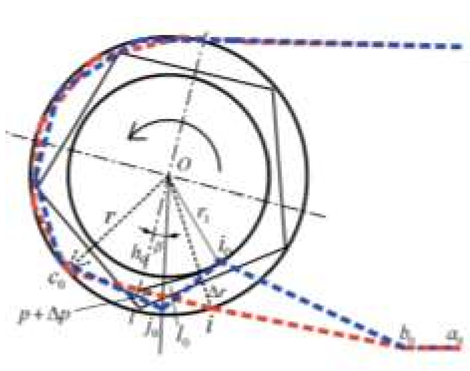

Figure 2: Meshing trajectory of five-gear sprocket

By analyzing the meshing trajectory combined with the triangular relationship, it can be obtained[13]:

$$\begin{cases}\dfrac{r_1^2+h^2-l_0^2}{2r_1h}=\cos\dfrac{90^\circ}{z}\\[2ex] \dfrac{\Delta r^2+\dfrac{(p+\Delta p)^2}{4}-l_0^2}{(\Delta p+p)\ \Delta r}=\sin\dfrac{90^\circ}{z}\\[2ex] h=\sqrt{4r^2-(p+\Delta p)^2}\,/\,2\\ r_1=r-\Delta r\end{cases} \quad (5)$$

Where Δr is the reduction of pitch circle radius, mm; r is the pitch circle radius, mm; p is the pitch of the scraper chain, mm; Δp is the increase of scraper chain pitch, mm; z is the number of sprocket teeth.

Then analyse velocity vector triangle at point i to obtain velocity variation:

$$\Delta v=\omega r_1\cos\left(\frac{90^\circ}{z}+\beta\right)-\omega r\cos\frac{90^\circ}{z} \quad (6)$$

With time variation $\Delta t=(90^\circ/z-\beta)/\omega$, the impact acceleration during meshing can be derived:

$$a_1=\frac{\omega^2(r-\Delta r)\cos\left(\frac{90^\circ}{z}+\beta\right)-\omega^2 r\cos\frac{90^\circ}{z}}{\frac{90^\circ}{z}-\beta} \quad (7)$$

3. Dynamics of Scraper Chain Drive

3.1 Calculation of Operating Resistance of Scraper Conveyor

The on-board short-distance swing-type scraper conveyor adopts a center-single-chain configuration, with its chain trough consisting of both straight and curved sections. During cyclic operation, the chain links and scrapers must alternately pass through these two distinct zones. To optimize conveyor design, particular emphasis must be placed on investigating the operational resistance characteristics of scrapers and chains under curved-path working conditions.

In practical operation, the running resistance of the scraper conveyor exhibits dynamic variation characteristics. This behavior can be attributed to two primary factors: firstly, the heterogeneous nature of transported materials, and secondly, the diverse installation configurations and drive modes employed. The combined influence of these factors results in distinct variation patterns of operational resistance during conveyor operation.

The on-board short-distance scraper conveyor system is illustrated in Figure 3, with the complete chain loop analysed in segmented sections:

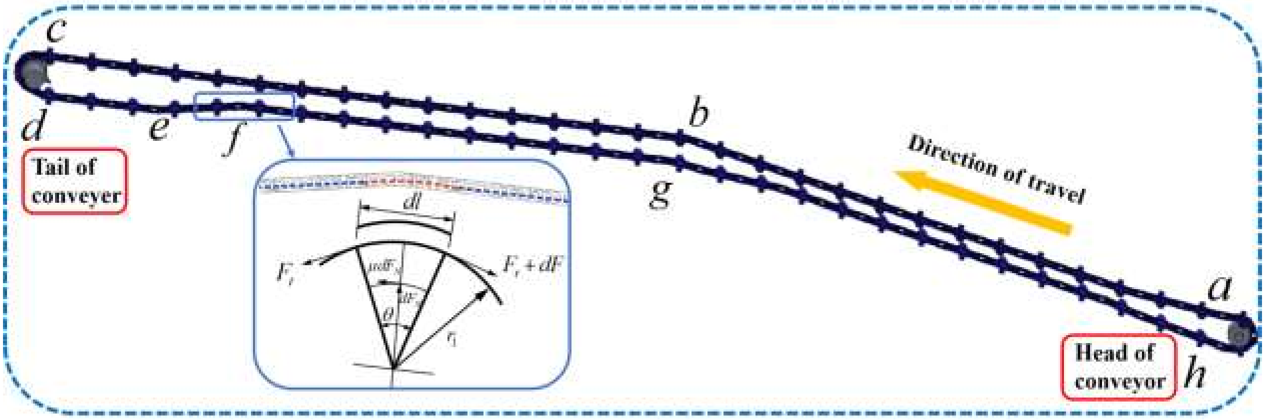

Figure 3: Analysis schematic diagram of the scraper conveying system

Analysis of resistance in the empty-load straight-section scraper chain conveying system was conducted. When the chain of the scraper conveyor operates under no-load conditions, the running resistances corresponding to the loaded strand *a-b-c* and empty return strand *d-e*、*f-g-h* of the scraper chain are as follows:

$$\begin{cases} W_z = q_0 Lg(c_0 \cos\beta_0 + \sin\beta_0) \\ W_k = q_0 Lg(c_0 \cos\beta_0 - \sin\beta_0) \end{cases} \tag{8}$$

Where q_0 is the mass per unit length of the scraper chain under no-load condition, kg/m; L is the length of the straight section of the scraper conveyor, m; g is the acceleration of gravity, m/s^2; c_0 is the friction resistance coefficient of the scraper chain running in the groove; β_0 is the transport dip, (°).

An analysis was conducted on the contact resistance between the scraper chain and the conveying chute in the curved section. Both the vertical curved portion *b, e, f, g* of the chain path and the redirection roller section *h-a* were modelled as circular arcs. Taking point *f* as an example, an arc segment of length *dl* was selected for analysis. The mechanical model and force analysis of the scraper chain micro-segment are illustrated in Figure 3. The force equilibrium in the vertical direction yields [9]:

$$\begin{cases} (F_t + dF)\cos\dfrac{d\theta}{2} - F_t\cos\dfrac{d\theta}{2} - \mu dF_N - F_z dl = 0 \\ (F_t + dF)\sin\dfrac{d\theta}{2} + F_t\sin\dfrac{d\theta}{2} - dF_N = 0 \end{cases} \tag{9}$$

When $d\theta$ infinitely approaches 0, it is simplified to:

$$\begin{cases} dF = \mu dF_N + F_z dl \\ dF_N = 2F\sin\dfrac{d\theta}{2} \approx Fd\theta \end{cases} \tag{10}$$

Given that $dl = r_1 d\theta$, the following relationship can be derived:

$$dF = F_z dl + \mu F_t d\theta = F_z r_1 d\theta + \mu F_t d\theta \tag{11}$$

Where F_z is the resistance per unit length of the scraper chain; μ is the friction factor; r_1 is the arc radius; F_t is the chain tension; F_N is the positive pressure; θ is the bend angle; l is the arc length.

Assuming that the tension at the contact between the chain and the arc section is F_2, and the tension of the chain after the bending angle is F_1, the differential equation can be solved under this boundary condition to obtain:

$$\int_{F_2}^{F_1} \frac{dF}{\mu F_t + F_z r} = \int_0^{\theta'} d\theta \tag{12}$$

Where F_1 is the tension at the starting point of the micro-segment scraper chain contacting the equivalent arc section, N; F_2 is the tension at the end point where the micro-segment scraper chain contacts the equivalent arc section, N; θ' is the arc bend angle, (°).

Since the friction force at the bending part of the actual scraper conveyor is only related to the positive pressure and friction factors it receives, and has nothing to do with the bending direction, the bending angle θ' can be replaced by the upper bending angle θ on the corresponding arc section length *dl*, i.e.: $r_1 = 1/\theta, \theta' = \theta l$, which is substituted into the formula (12), and then the tension of the equivalent arc section of the micro-segment scraper chain is calculated as[6]:

$$F_2 = F_1 e^{\mu\theta l} + \frac{F_z}{\mu\theta}(e^{\mu\theta l} - 1) \tag{13}$$

Substitute *l*=*L*, the chain tension applied to the chain plate on the scraper conveyor can be expressed as:

$$\begin{cases} F_{s1} = F_{s2}e^{\mu\theta L} + \dfrac{F_{z'}r_s}{\mu}(e^{\mu\theta L} - 1) \\ F_{z'} = q_0 g(c_1 \cos\beta_0 \pm \sin\beta_0) \end{cases} \tag{14}$$

Then solve Eq. (14) to obtain the following:

$$F_{s1} = F_{s2}e^{\mu\theta L} + \frac{q_0 g r_s(c_1 \cos\beta_0 \pm \sin\beta_0)}{\mu}(e^{\mu\theta L} - 1) \tag{15}$$

Where F_{s1} is the upper chain tension after the scraper chain is bent, N; F_{s2} is the upper chain tension at the initial bending point of the scraper chain, N; $F_{z'}$ is the resistance per unit length of the upper scraper chain; L is the length of the upper chain arc section of the scraper conveyor, m; c_1 is the friction resistance coefficient of the scraper chain in the upper chain path; r_s is the corresponding equivalent arc radius of the bending section of the upper chain, m.

Similarly, the tension of the lower chain can be expressed as:

$$F_{x1} = F_{x2}e^{\mu\theta L_0} + \frac{\mu q_0 g c_2 r_x \sin 2\beta_0}{2\mu}(e^{\mu\theta L_0} - 1) \tag{16}$$

Where F_{x1} is the lower chain tension after the scraper chain is bent, N; F_{x2} is the lower chain tension at the initial bending point of the scraper chain, N; L_0 is the length of the lower chain arc section of the scraper conveyor, m; c_2 is the friction resistance coefficient of the scraper chain in the lower chain path; r_x is the corresponding equivalent arc radius of the bending section of the lower chain, m.

Similarly, the tension at any point of contact between the scraper chain and the corresponding arc section of the turnabout roller can be expressed as:

$$F_{l1} = F_{l2}e^{\mu\theta L_1} + \frac{q_0 g r_l(c_3 \cos\beta_0 \pm \sin\theta L_1)}{\mu}(e^{\mu\theta L_1} - 1) \tag{17}$$

Where F_{l1} is the tension after the scraper chain is bent out of the roller, N; F_{l2} is the tension of the scraper chain bending into the initial point of the roller, N; F_{z1} is the resistance per unit length of the scraper chain; L_1 is the length of corresponding arc section of scraper chain and roller, m; c_2 is the friction resistance coefficient of the scraper chain roller; r_l is the corresponding equivalent arc radius of the bending section of the roller, m.

Subtract the initial point tension force F_{s2}, F_{x2} and F_{l2} respectively from Equation (15) (16) (17) to obtain the drag force at the upper and lower chains of the curved scraper and the drag force at the bend roller:

$$\begin{cases} W_s = F_{s1} - F_{s2} = \left[F_{s2} + \dfrac{q_0 g r_s(c_1 \cos\beta_0 \pm \sin\beta_0)}{\mu}\right](e^{\mu\theta L} - 1) \\ W_x = F_{x1} - F_{x2} = \left[F_{x2} + \dfrac{\mu q_0 g c_2 r_x \sin 2\beta_0}{2\mu}\right](e^{\mu\theta L_0} - 1) \\ W_l = F_{l1} - F_{l2} = \left[F_{l2} + \dfrac{q_0 g r_l(c_3 \cos\beta_0 \pm \sin\theta L_1)}{\mu}\right](e^{\mu\theta L_1} - 1) \end{cases} \tag{18}$$

When analysing additional resistance during conveyor chain operation, the supplementary resistance is calculated as 10% of the straight-section running resistance [8], expressed as:

$$W_f = 0.1(W_z + W_k) \tag{19}$$

From the above computational analysis of the operational resistance in the airborne short-stroke swing conveyor, it is evident that the current approach primarily involves direct summation of individual resistance components. However, this methodology fails to account for the complex interactions among internal system elements. Furthermore, existing analytical methods exhibit notable limitations in both computational and interpretative aspects when addressing dynamic load-induced resistance variations, rendering them inadequate for accurately characterizing real-world operational resistance dynamics.

3.2 Analysis of the Running Resistance of Chain in Bending Section under Different Driving Modes

The running resistance of the bending section chain of the conveyor is composed of upper chain, lower chain and turnabout roller. Due to the different arrangement of the driving device, the chain tension distribution will be different, thus affecting the running resistance of the upper and lower scraper chains. The following analyses the operating resistance in two driving modes.

Head drive, upper and lower chain plate resistance:

$$F'_{oL} = \frac{q_0 g(c_1 \cos\beta_0 \pm \sin\beta_0)}{\mu\theta}(e^{\mu\theta L} - 1) \tag{20}$$

$$F'_{uL} = \frac{(e^{\mu\theta L} - 1)}{\mu\theta}\begin{bmatrix} q_0 g(c_1 \cos\beta_0 \pm \sin\beta_0)\ (e^{\mu\theta L} - 1) \\ +\dfrac{1}{2}\mu q_0 g c_2 \sin 2\beta_0 \end{bmatrix} \tag{21}$$

Tail drive, upper and lower chain plate resistance:

$$F'_{oL} = \frac{(e^{\mu\theta L} - 1)}{\mu\theta}\begin{bmatrix} q_0 g(c_1 \cos\beta_0 \pm \sin\beta_0) + \\ \dfrac{1}{2}\mu q_0 g c_2 \sin 2\beta_0(e^{\mu\theta L} - 1) \end{bmatrix} \tag{22}$$

$$F'_{uL} = \frac{\mu q_0 g c_2 \sin 2\beta_0}{2\mu\theta}(e^{\mu\theta L} - 1) \tag{23}$$

The total bending section resistance under each driving mode can be obtained by combining the upper and lower chain resistance formulas of each driving mode with the bending section formula of the corresponding roller.

3.3 Torque Calculation of Drive Sprocket of Conveying System

Based on the analysis on the chain transmission structure of the intermediate single-chain short-distance scraper conveyor, the roller chain bypasses the drive sprocket from the upper chain plate, passes through the lower chain plate, bypasses the turnabout roller, and then turns to the upper chain plate. The chain is only engaged with the drive sprocket teeth to transmit motion and force. As shown in Figure. 3, the types of sections where the scraper chain passes through are different. The driving force required for the whole cycle of scraper chain operation can be obtained by superposition of the running resistance of the scraper chain in each section:

$$\begin{cases} W_1 = \sum W_s + \sum W_x + W_l + W_f \\ T = W_1 / R \end{cases} \tag{24}$$

Where $\sum W_s$ is the sum of the running resistance of the upper chain plate of each section, N; $\sum W_x$ is the sum of the running resistance of the lower chain plate of each section, N; T is the torque required by the drive sprocket, $N \times m$;R is the theoretical dividing circle radius of the driving sprocket, m.

4. Modelling and Simulation Setup

4.1 Conveyor Position Distribution and Model Building

Based on the physical on-board short-distance scraper conveyor equipped on the roadheader-bolter combination, a 3D model was established using SolidWorks software, as specifically illustrated in Figure 4. The key technical parameters of major components are listed in Table 1. The complete solid model was simplified and then imported into the multibody dynamics simulation software RecurDyn in .x_t file format, with consistent conveyor orientation maintained to ensure uniform gravity direction.

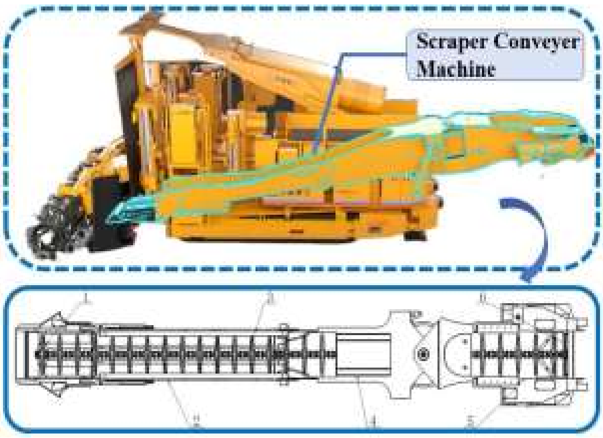

1.turnabout roller 2. front transport trough 3. scraper chain assembly 4. middle transport trough 5. conveyor tail 6. drive sprocket

Figure 4: Modeling model of the on-board short-distance swinging scraper conveyor

Table 1. Main technical parameters of key components

Parameter	Value
Working face length	9520 mm
Chute width	770 mm
Scraper spacing	325.15 mm
Chain pitch	81.3 mm
Chute depth	267.5 mm

4.2 Tension of Scraper Chain in two Drive Modes

This paper analyzes the operational principle of the on-board short-distance scraper conveyor in excavation-anchoring integrated equipment. The conveyor structure is simplified by retaining only the middle trough and tail section, with the front end redesigned based on the redirection roller configuration, ensuring no impact on simulation accuracy.

Two drive models are defined:

Head drive mode: A hydraulic cylinder adjusts tail roller position to control chain tension, mimicking the pre-operation expansion/contraction mechanism of continuous miners.

Tail drive mode: A hydraulic cylinder actuates a compensation slide plate integrated with the drive assembly to regulate sprocket shaft position, replicating the tensioning system of excavation-anchoring equipment.

In the virtual prototype, chain tension is achieved by applying axial displacement drives to the tail sprocket shaft and slide plate assembly. After proper tensioning, rotational drive is initiated at the drive sprocket to ensure stable operation without chain accumulation (Figure. 5).

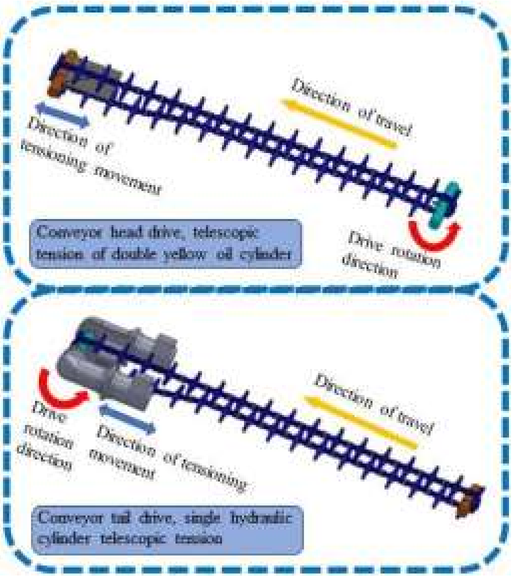

Figure 5: Dynamic tensioning diagram of the on-board short-distance scraper conveying system

4.3 Simulation Model Setting

The main contact settings for the simulation are listed in Table 2. All components of the scraper conveyor are modelled with low-carbon steel material properties, featuring a density of 7.8×10^{-6} kg/mm^3.

Table 2. Main contact settings for virtual prototypes

Parameter	Value
Stiffness factor	10000 N/mm
Damping coefficient	100 N·s/mm
Young's modulus	200000 N/mm^2
Rolling friction coefficient	0.25
Static friction coefficient	0.3
Stiffness factor	2
Poisson's ratio	0.3

The simulation setting of the topological structure between the components of the scraper conveyor is shown in Figure 6.

Figure 6: Topological structure relationship diagram

Referring to the actual working conditions of the on-board short-distance scraper conveyor, the boundary conditions for the tensioning motion of the scraper chain and the drive sprocket movement under two driving modes are established, as listed in Table 3.

Table 3. Definition of driving function and displacement function

Type of drive	Head-Driven	Tail-Driven
Tensioning displacement function	STEP (TIME,0,0,0.5, ±25)	
Drive sprocket speed function	STEP (TIME, 0.5,0,2.5, ±7.8)	STEP (TIME, 0.5,0,2.5, ±10.7)
	STEP (TIME, 0.5,0,2.5, ±13.3)	STEP (TIME, 0.5,0,2.5, ±15.8)

The tensioning function of the conveyor is achieved through displacement function expressions. Taking STEP (TIME, 0, 0, 0.5, ±25) as an example, this indicates that the initial position of the tensioning slide is zero at startup. After 0.5 s, it reaches the rated displacement of 25 mm, completing the tensioning process.

Subsequently, the motion drive in TraJoint is activated. The movement of the drive sprocket under various load conditions is controlled by velocity function expressions to regulate chain speed variations. For instance, STEP (TIME, 0.5, 0, 2.5, ±15.8) denotes that the drive sprocket maintains an initial speed of zero for the first 0.5 s and accelerates to the rated operating speed of 15.8 rad/s (corresponding to a chain speed of 2.1 m/s) by 2.5 s

5. Simulation Test Analysis

The virtual prototype models of the two driving modes of the mid-single-chain short-distance scraper conveying system are shown in Figure.7. The chain in the meshing area of the drive sprocket in different modes are marked with corresponding section numbers. In this paper, the scraper in the head driving mode No.16 and the scraper in the tail driving mode No.27 are selected as the research objects to analyse the dynamic contact characteristics at the meshing of the sprocket; As the scraper of head drive mode No.16 and the scraper of tail drive mode No.9 have similar geometric positions, it is selected as the research object to analyse the dynamic characteristics of drive sprocket during the periodic contact of conveying system.

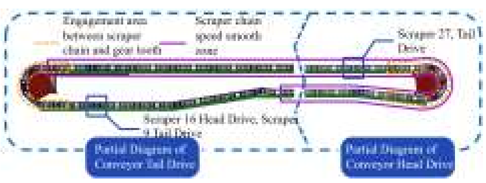

Figure 7: Schematic diagram of the local model of the virtual prototype of the two drive schemes

Based on incomplete statistics regarding the conveying inclination and chain speed of the continuous miner haulage system used in Shendong Mining Area of China Energy Group, the conveying inclination (ranging from 0° to 12°) and the scraper chain speed were selected as experimental variables. Accordingly, 24 working conditions were defined, with specific numbering as shown in Table 2-4.

Table 4. Table of simulation working condition numbers

Condition number		Head-Driven			Tail-Driven		
dip angle/ (°)		0		8			12
chain speed v/(m · s^{-1})	0.9	1	2	3	13	14	15
	1.3	4	5	6	16	17	18
	1.7	7	8	9	19	20	21
	2.1	10	11	12	22	23	24

5.1 Influence of Conveying Inclination on Acceleration Impact of Different Driving Modes

Figure 8 presents a comparative analysis of chain-sprocket interaction characteristics under two different drive configurations, with the conveyor operating at a constant chain speed of 2.1 m/s. The analysis specifically examines three operational scenarios corresponding to conveyor inclination angles of 0°, 8°, and 12°.Among them, the scraper chains of each research object run in the chain channel completely for one week, and the simulation test takes 7.5 s.

Figure.8 (a) shows the acceleration change state during the interaction between the #16 scraper chain and the drive sprocket in the head driving mode. The #16 scraper engages the teeth from 3.6s and meshes out at 4.0s. Operating condition 10 obviously shows that the acceleration of the scraper increases significantly and reaches the maximum value of 42.5m/s^2 in the meshing process when the chain wheel turns to 234°~297°, When the gear teeth rotate 360° and cycle again to 126°, the acceleration fluctuation gradually decreases. Figure.8 (b) Under the tail drive mode, the scraper chain is located at the chain wheel corner 72°, i.e. the instantaneous acceleration impact at the gear teeth meshing chain increases to the maximum, and the acceleration impact gradually decreases to 15m/s^2 between the corner 72°~324° Below. The acceleration impact on the chain will increase with the increase of the angle when the inclination angles of working conditions 22,23 and 24 are increased; In the tail drive mode, the acceleration impact of the scraper chain is slightly influenced by the tilt angle.

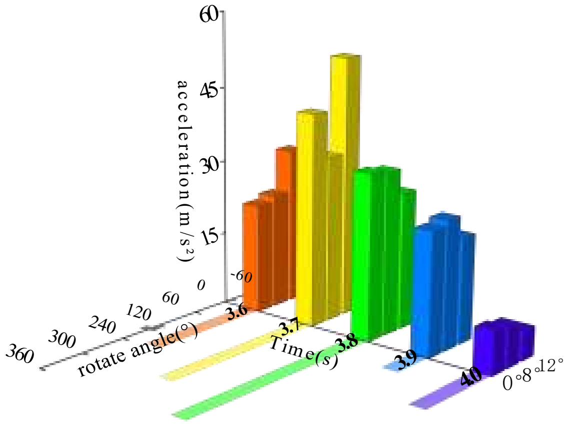

(a) No.16 scraper chain enters engagement zone of front drive sprocket

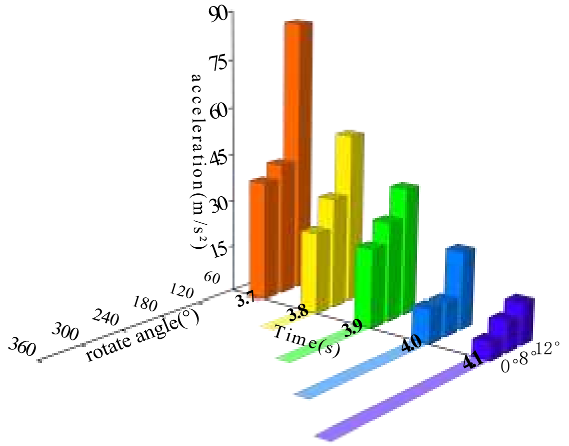

(b) No.27 scraper chain enters engagement zone of rear drive sprocket

Figure 8: Impact characteristics of acceleration at various inclination angles

5.2 Influence of Conveying Inclination on Dynamic Change of Chain Wheel Torque under Different Driving Modes

The scraper chain of the conveyor is in the accelerating stage within 0~2.5s, and the #16 and #9 scrapers are located in the accelerating area of the initial position of the lower chain. Figure.9(a) The scraper runs to the fixed speed area within 2.5s~7.5s and cycles for a whole cycle. Under working condition 11, during the operation of the scraper, the driving torque of the drive sprocket changes in wave pattern. The driving torque decreases from 385 N·m to 260 N·m and then increases to 430 N m, which reciprocates, and the value fluctuates. The overall analysis from working conditions 10,11 and 12 shows that the dip angle increases, and the fluctuation peak value increases accordingly. Figure.9(b) Operating condition 22 increases the driving torque of the tail drive sprocket linearly within 3.9s~4.4s during the operation of scraper 9 and then drops back to the minimum driving torque in a short sudden change. The torque changes periodically during the operation.

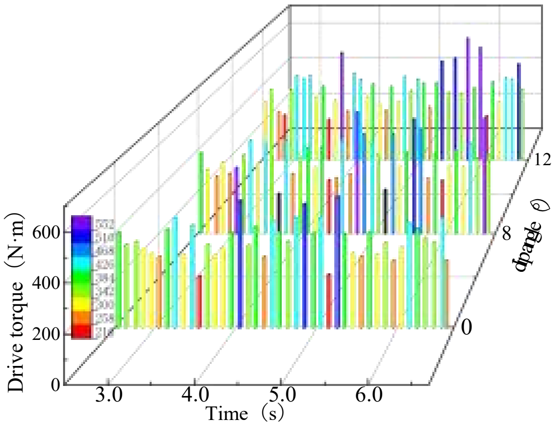

(a) No.16 scraper chain reaches constant-speed section

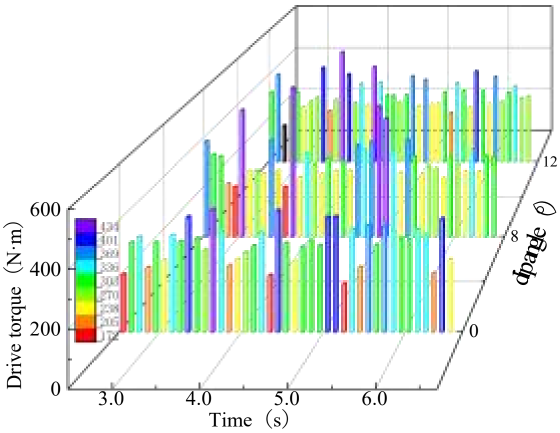

(b) No.9 scraper chain reaches constant-speed section

Figure 7: Dynamic torque characteristics of sprockets at various conveying inclinations

5.3 Impact of Chain Speed on Acceleration Shock in Different Drive Modes

Figure.10 shows the analysis on the acceleration state of the engagement between the scraper chain and the drive sprocket under the four states of scraper chain speed of 0.9 m/s, 1.3 m/s, 1.7 m/s and 2.1 m/s, taking the conveying inclination of 12 ° as an example. Among them, the #16 and #27 scraper chains in the research object run for one complete week in the upper and lower chain channels, and the simulation test time of four chain speeds is 13.5s, 10.5s, 8.7s and 7.5s respectively.

Figure.10(a) Under the driving mode of head, when the relative displacement is -0.3~0.3m, it can be obviously observed that the acceleration curve in the process of chain engagement is very large at first and then gradually reduced. The maximum acceleration occurs at the relative displacement of -0.15 m at the gear teeth fully engaged with the chain, and the peak value is 28 m/s^2 and 37 m/s^2. In working condition 8, the chain suddenly changes when engaging the gear tooth, so the peak value is 33.4 m/s at -0.35m^2 This affects the subsequent engagement. The trend of condition 11 is approximately the same as that of condition 8, but the sudden change is obvious, and the peak acceleration impact of the scraper reaches 60.2 m/s^2. Figure.10(b) Under the tail drive mode, with the increase of chain speed, the overall trend of acceleration impact becomes more obvious, and the chain speed has a greater impact on it. The sudden change peak value of meshing appears at the position of -0.25m under working condition 21 and working condition 24, and the value is 73 m/s^2 and 86.5 m/s^2。 When the chain is meshed out and enters the lower chain channel, the acceleration impact is obviously weakened and tends to be stable.

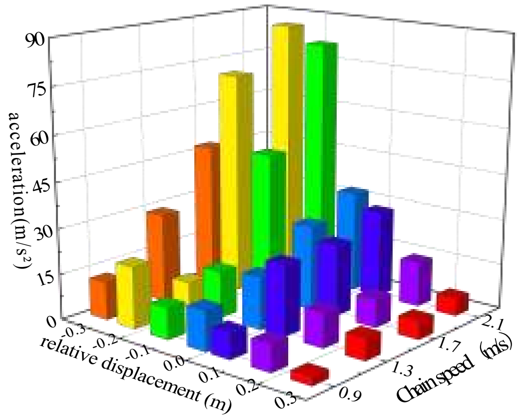

(a) Engagement area of #16 scraper chain and chain wheel

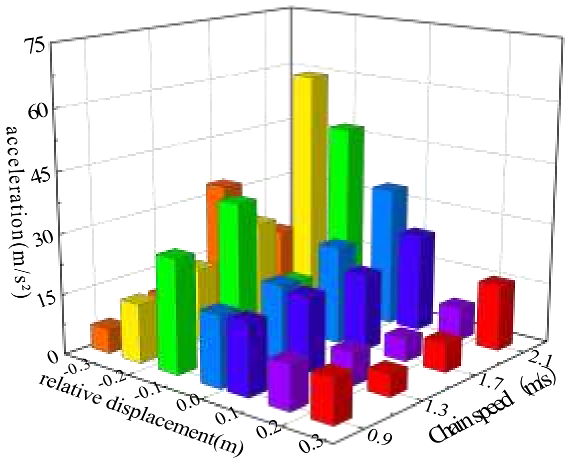

(b) Engagement area of #27 scraper chain and chain wheel

Figure 10: State curve of acceleration of scraper chain running to contact with drive chain wheel at similar relative positions of different chain speeds

5.4 Effect of Chain Speed on Dynamic Sprocket Torque Variations in Different Drive Modes

Figure.11 shows the dynamic change rule analysis of drive sprocket torque when the scraper runs to the fixed speed area in the whole cycle under the four states of scraper chain speed of 0.9 m/s, 1.3 m/s, 1.7 m/s and 2.1 m/s, taking the conveying inclination of 12° as an example.

Figure.11 Dynamic driving torque variation trend of chain wheel shows pentagonal star fluctuation variation law during the whole cycle operation. Figure.11(a) The driving torque of the drive sprocket changes significantly when operating at 0°~30° and 210°~230° under working condition 2, and the peak value of the change point is 975.3 N·m. When the chain speed increases, the driving torque value under condition 8 of Figure.11(b) fluctuates greatly.

When the chain engages in and out of the teeth of the five-tooth sprocket, the torque fluctuates, a sudden change point occurs at an interval of 72 °, and the peak value reaches 1270 N·m. Figure.11(c) Under condition 11, the sudden change point of driving torque increases significantly, and the peak value also increases with the increase of chain speed. The value exceeds 1530 N·m at many places, and the torque fluctuation shows obvious pentagram alternating phenomenon. Figure.11(d) (e) (f) The fluctuation trend of sprocket driving torque in the tail drive mode under the corresponding chain speeds of Condition 15, Condition 21 and Condition 24 is similar to that of the head drive mode. The maximum sudden change value is at 89.9° of the sprocket angles under Condition 24, and the peak value is 1085.5 N·m. The numerical distribution is relatively uniform.

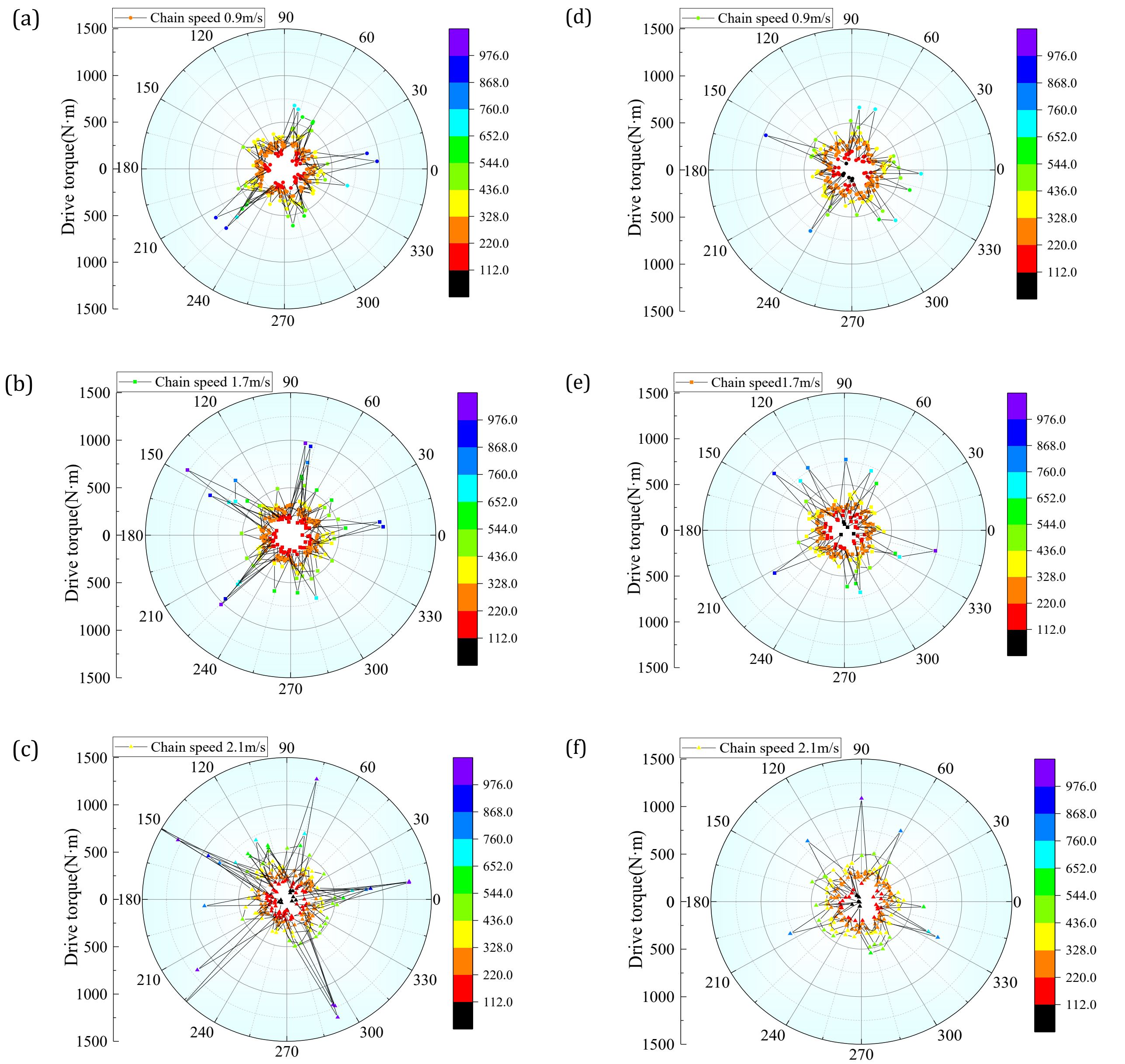

(a-c) Head drive chain speed 0.9m/s,1.7m/s, 2.1m/s; (d-f) Tail drive chain speed 0.9m/s,1.7m/s, 2.1m/s

Figure 11: Distribution patterns of driving torque on sprockets at various chain speeds

6. Comparison and Discussion of Results

6.1 Comparative Analysis of Operational Characteristics at Different Conveying Inclinations

Figure. 8 (a) In the first 0.2s of the engagement process in the nose drive mode, the chain link is removed from the lower chain plate and contacts the five-tooth sprocket for interaction. Due to the influence of polygon, the chain link rotates from the lowest engagement point β angle to the highest point, and the acceleration a_1 rapidly increases to the maximum. Currently, the chain pitch increases, and the chain is completely engaged after a short time. The relative static of the gear teeth and the chain link only changes with the rotation angle, and the acceleration impact drops rapidly; Figure.8 (b) The chain link of tail drive mode is moved out from the upper chain plate and engaged into the five-tooth chain wheel. The tooth tip contacts the chain link to produce acceleration change. With the increase of conveyor inclination β_0, the acceleration impact is positively correlated with the inclination, indicating that the smaller the inclination is, the smaller the impact on the gear teeth will be; The two modes have different peak acceleration positions, where the polygon effect is obvious, but the average value shows that the head drive mode is slightly less affected by the tilt angle than the tail drive mode.

Figure.9 (a) When the conveyor is accelerated to the rated speed, the driving torque of the tail changes into the wave fluctuation law, which is caused by the sudden increase of the chain tension F_t when the scraper chain is wound into the drive sprocket through the lower chain plate, resulting in a temporary sudden change of the operating resistance W_l when it is in contact, while when it is wound out of the gear tooth, the tension Ft gradually decreases with the increase of the tilt angle β_0, thus affecting the driving torque T, The collision becomes more obvious and moves quickly to plateau when the inclination is larger at the moment of contact. Figure 9 (b) When the tail drive mode is adopted, the operating resistance F_{ol}' and F_{ul}' of W_1 sudden change and bending section at the roller are different from the head drive mode to affect the driving torque T, and the average value is smaller than the head drive mode.

6.2 Comparative Analysis of State Characteristics of Different Chain Speeds

Figure.10 (a) clearly shows that when the scraper chain runs to the engagement area, the acceleration impact distribution trends of 0.9 m/s, 1.3 m/s, 1.7 m/s and 2.1 m/s for the same drive mode are approximately the same, while the higher the chain speed is, the more obvious the collision between the chain link and the sprocket is when engaging, indicating that the acceleration impact a_1 caused by the polygon effect here is large, and the instability coefficient K_t is also large. Figure.10 (b) shows that the acceleration impact of the tail drive mode in the meshing area is greater than that of the head drive mode, and the chain speed v is controlled by the five-tooth sprocket speed ω, so the rotation speed ω is positively correlated with the acceleration a_1. Therefore, the service life of the chain wheel can be increased by selecting the appropriate chain speed under the condition of meeting the transport capacity.

Figure.11 (a)~(c) shows that under the nose drive mode, the increase of chain speed has a particularly significant impact on the driving torque, and the fluctuation presents a pentagonal change. This phenomenon is determined by the number of sprocket teeth. The five-tooth sprocket generates a chain pitch change Δp under the polygon effect of 72 ° rotation, making the chain tension F_t fluctuate, and finally a peak appears. The higher the chain speed is, the greater the peak value is. At the same time, there is an inertial load to reduce the corresponding trough value, the uneven impact collision is obvious, and the tooth wear is serious. Figure.11 (d)~(f) shows that in the tail drive mode, the driving torque mutation change trend is similar to the nose drive mode, but the influence of chain speed on it is weakened obviously. Under each chain speed, the torque value is evenly distributed, and the impact reduction on the power output shaft is obviously better than the nose drive mode, thus reducing the fault rate of the reducer gear and the motor.

7. Conclusions

This article studies the dynamic characteristics of the on-board short-distance scraper conveyor under two driving modes, and the main conclusions are as follows:

(1) When the dip angle of the conveyor changes, the acceleration impact load and the dip angle show a positive correlation law, that is, the smaller the dip angle is, the smaller the impact on the gear teeth is, and the impact is affected by the polygon effect; Through the comparison and analysis of the two driving modes, the head drive is slightly less affected by the tilt angle than the tail drive. When the conveyor accelerates to the rated speed, the tail driving torque changes into wave fluctuation law, and the driving torque is greatly affected by the running resistance, so the tail driving is better than the head driving.

(2) With the increase of chain speed, the acceleration impact caused by polygon effect intensifies, showing a positive correlation with the instability coefficient; The change of chain speed has

a significant impact on the driving torque, and the numerical fluctuation shows a "pentagonal star" change law; The regular change is determined by the number of sprocket teeth, z, and the five-tooth sprocket produces impact fluctuation when engaged with the chain link every 72 ° rotation; Sudden change of driving torque under head driving mode is much greater than that under tail driving mode.

(3) Through the comparative analysis of two modes of head-drive and tail-drive, under the same conveying inclination and scraper chain speed, the tail-drive can effectively suppress the impact caused by sudden change of torque and make the dynamic change of torque more uniform and then improve the overall transportation performance of short-distance scraper conveyor of coal mining equipment.

Acknowledgments

This work was sponsored by the Fund for National Natural Science Foundation of China (Grant No.52475117) and Fundamental Research Program of Shanxi Province (Grant No.202403021211072) and Central Guidance for Local Scientific and Technological Development Fund (Grant No. YDZJSX20231A050).

Declaration of conflicting interests

The authors declare that they have no known competing financial interests or personal relationships that could have appeared to influence the work reported in this paper.

References

[1] Gao, A.H. (2016) Analysis of Meshing Characteristics of Chain Drive of Short-distance Heavy-duty Scraper Conveyor. Coal Engineering, 48(04):135-138. https://link.cnki.net/urlid/11.4658.TD.20160527.0949.080

[2] Guo, J.B. (2022). Research and application of low noise chain drive system in swing scraper conveyor. Coal technology,41(12):215-218. https://link.cnki.net/doi/10.13301/j.cnki.ct.2022.12.050

[3] He H. B. (2024). Wear resistance of chain rings of scraper conveyor under different abrasive conditions. Coal Engineering. 56(07):213-219. https://www.chinacaj.net/MKSJ/doi/10.11799/ce202407032

[4] Jiang, L. Y. (2007). Design of mine airborne short-distance scraper conveyor. Coal mine machinery, (05):1-3.https://link.cnki.net/doi/10.13436/j.mkjx.2007.05.001

[5] Ma H. Z., Wang X. W., Li B. (2022). Study on the mechanical effect and wear behavior of middle trough of a scraper conveyor based on DEM-MBD. Proceedings of the Institution of Mechanical Engineers, Part J: Journal of Engineering Tribology, 236 (7):1363-1374. https://doi.org/10.1177/13506501211059259

[6] Mao, J., Zhang, Y.S., Xie, C.X. (2022). Torsional vibration mechanical model construction of scraper conveyor and working condition analysis of over bending section. Mechanical strength, 44 (02): 279-286. https://link.cnki.net/doi/10.16579/j.issn.1001.9669.2022.02.004

[7] Song, W. J., Jing, Q. H., Zhang, H.Q. (2023). Study on Mechanical Properties of Scraper Conveyor under Bending Section Condition. Coal Technology,42(11):221-225. https://link.cnki.net/doi/10.13301/j.cnki.ct.2023.11.048

[8] Sheehy DJ. (2003). Balance of melty-drive convey motors with wound rotor motors. Bulk Solids and ling,23(3):182-185. https://www.researchgate.net/publication/293496345

[9] Wang, X. W., Wang, S. P., Long, R. S. (2016). Analysis of rigid-flexible coupling contact dynamic characteristics of heavy scraper conveyor chain drive system load start-up. Vibration and impact,35(11): 34-40. https://link.cnki.net/doi/10.13465/j.cnki.jvs.2016.11.006

[10] Wang, K., Li, Y., Tian, N. (2022). Dynamic characteristics of roller chain under high-speed continuous strong impact. Vibration and impact,41(15):280-286. https://link.cnki.net/doi/10.13465/j.cnki.jvs.2022.15.035

[11] Wang W., Zhang T., Yang W Q. (2024). Dynamics modeling and vibration failure analysis of a rigid-flexible coupled chain meshing drive system. Journal of Vibration and Shock,43(18):278-286. https://jvs.sjtu.edu.cn/CN/Y2024/V43/I18/278

[12] Wang, Y., Li, J.X., Wang, J.X. (2019). Study on impact characteristics of middle trough of scraper conveyor. Industrial and mining automation, 45(04): 19-23+29. https://link.cnki.net/doi/10.13272/j.issn.1671-251x.2018120073

[13] Yang, L., Zhang, H., Song, Y. (2023). Study on multibody contact load distribution characteristics of scraper conveying system of continuous miner. Transactions of the Canadian Society for Mechanical Engineering,47(4): 575-587. https://doi.org/10.1139/tcsme-2023-0017

[14] Zhang, Y. L., Wang, B. K., Zhang, X. (2021). Forty years 'development and future prospect on mechanized short-wall mining technology with continuous miner in China. Journal of China Coal Society, 46,86-99, https://link.cnki.net/doi/10.13225/j.cnki.jccs.2020.1632

[15] Zhao, X. Y. (2023). Study on impact wear of middle trough of scraper conveyor based on different dip angles. Industrial and mining automation, 49(S1):63-66+85.

[16] Zhang, B. (2020). Calculation and derivation of the resistance of scraper conveyor chain operation. Electromechanical engineering technology,49(03):67-68. https://d.wanfangdata.com.cn/periodical/jxkf202003033